

## Experimental and CFD studies of a thermoacoustic apparatus

W. T. Lee<sup>1</sup>, F. A. Z. Mohd Saat<sup>1,2\*</sup>

<sup>1</sup>Fakulti Kejuruteraan Mekanikal, Universiti Teknikal Malaysia Melaka, Hang Tuah Jaya, 76100 Durian Tunggal, Melaka, Malaysia.

<sup>2</sup>Centre for Advanced Research on Energy, Universiti Teknikal Malaysia Melaka, Hang Tuah Jaya, 76100 Durian Tunggal, Melaka, Malaysia.

### ABSTRACT

*This paper reports a study of a thermoacoustic system by both experimentation and simulation works. A small scale thermoacoustic prototype was built for experimentation purposes. The prototype was built based on a thermoacoustic cooler setup. In addition, a two-dimensional transient thermoacoustic model was solved by using computational fluid dynamics (CFD) software. In experimentation, a small thermoacoustic rig operated at a frequency of 133.45 Hz was built and the system was tested using two different types of stack; acrylonitrile butadiene styrene (ABS) and a stainless-steel scrubber. At atmospheric pressure and at a relatively low frequency, a small temperature drop of approximately 1°C was recorded. Similar result (with an error of 0.1%) was obtained using a simple CFD model that was designed based on the actual operating parameters of the experimental rig with ABS as a stack. The study shows that thermoacoustic principles can be achieved using simple experimental as well as numerical setups. Future works are focussing on optimising the apparatus so that better performance can be achieved. In optimised condition, thermoacoustic principle can create a sustainable and green alternative technology for a refrigerator or an engine.*

**KEYWORDS:** Thermoacoustic; Computational Fluid Dynamics (CFD); temperature difference; temperature drop

### 1.0 INTRODUCTION

Thermoacoustic is a study that focuses on the interaction between thermodynamic and acoustic which are about the energy conversion from sound kinetic to heat (thermoacoustic refrigerator) or heat to sound kinetic (thermoacoustic engine) (Ibrahim et al., 2011). Figure 1 shows a schematic diagram of a thermoacoustic cycle on how the air particles in a thermoacoustic stack perform heat transfer (Dyatmika et al., 2015).

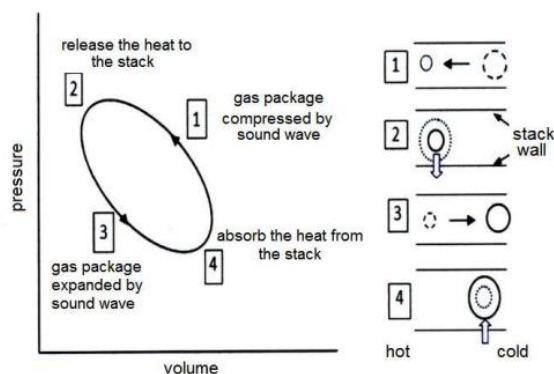


Figure 1: Schematic Diagram of Thermoacoustic Cycle (Dyatmika et al., 2015)

The objectives of this research are to design a small scale thermoacoustic prototype for experimentation, test the small scale thermoacoustic system using suitable measurement method, and model a simple thermoacoustic flow field by using Computational Fluid Dynamics (CFD) software. This research focuses only on the temperature at both ends of a structure known as ‘stack’ at certain pressure and velocity conditions inside a thermoacoustic refrigeration laboratory setup.

Some formulas and terminologies should be understood to investigate the flow in a thermoacoustic system. Generally, there are few terminologies and formulas that are important in thermoacoustic system such as wavelength of sound,  $\lambda$  in Equation (1), thermal penetration depth,  $\delta_k$  in Equation (2), viscous penetration depth,  $\delta_v$  in Equation (3) while the square of the viscous penetration depth divided by thermal penetration depth is equivalent to Prandtl number,  $\sigma$  as shown in Equation (4) (Swift, 2001).

$$\lambda = a / f \quad (1)$$

$$\delta_k = \sqrt{2k / \omega \rho C_p} = \sqrt{2\kappa / \omega} \quad (2)$$

$$\delta_v = \sqrt{2\mu / \omega \rho} = \sqrt{2\nu / \omega} \quad (3)$$

$$\left( \frac{\delta_v}{\delta_k} \right)^2 = \frac{\mu C_p}{\kappa} = \sigma \leq 1 \quad (4)$$

where  $a$  is speed of sound,  $f$  is oscillation of frequency,  $k$  is thermal conductivity,  $\omega$  is angular frequency which is equivalent to  $2\pi f$ ,  $\rho$  is density of gas,  $C_p$  is specific heat per unit mass at constant pressure,  $\kappa$  is diffusivity of the gas,  $\mu$  is gas dynamic viscosity, and  $\nu$  is gas kinematic viscosity. Equation (1-4) are used to determine the fundamental parameters for thermoacoustic refrigerator.

The inlet pressure and mass flux equations are as shown in Equation (5) and Equation (6) (Mohd Saat & Jaworski., 2013). Equation (5) and Equation (6) are interpreted in the Computational Fluid Dynamics (CFD) for the inlet pressure and mass flux. They are also used to find the theoretical velocity of the flow and to validate the simulation result.

$$P_1 = P_a \cos(Jx) \cos(2\pi ft) \quad (5)$$

$$m_1 = (P_a / c) \sin(Jx) \cos(2\pi ft + \theta) \quad (6)$$

where  $P_1$  is the inlet pressure,  $P_a$  is the antinode pressure,  $J$  is the wave number,  $x$  is the length of the resonator,  $f$  is the frequency of flowing air,  $t$  is the time taken,  $\theta$  is the phase difference, and  $m_1$  is the mass flux.

Since the acrylonitrile butadiene styrene (ABS) stack is usually made by CubePro 3D printer, it is necessary to understand its printing setup in order to obtain a good quality ABS stack. It is found that the shorter the layer thickness, the greater the interlayer bonding but product printed by 200  $\mu\text{m}$  layer thickness produces reasonable mechanical response because the strength of long flat plateau is good (Rosli et al, 2017).

Figure 2 shows the build setting of a CubePro Software.

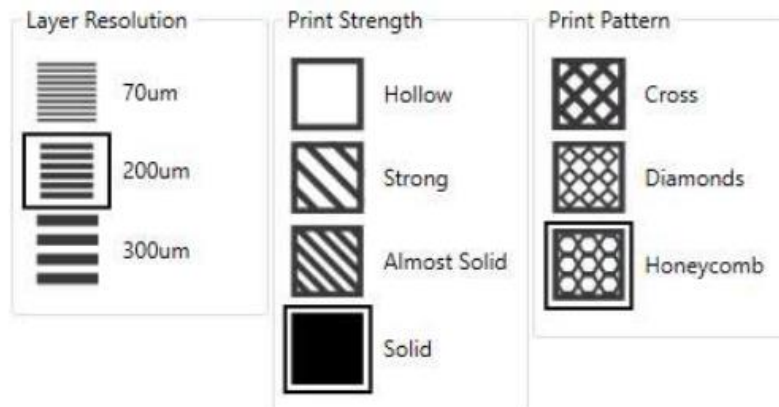


Figure 2: Build Settings of CubePro Software

## 2.0 METHODOLOGY

This research works consist of both experimentation and simulation analyses and the methodology for experimentation and simulation are discussed in subsection 2.1 and subsection 2.2 respectively.

### 2.1 Experimentation

To study the flow inside thermoacoustic system, an simple experimental rig of thermoacoustic refrigerator is built. Figure 3 shows a schematic diagram thermoacoustic refrigerator while Figure 4 shows the experimental rig of thermoacoustic refrigerator that is built in the laboratory.

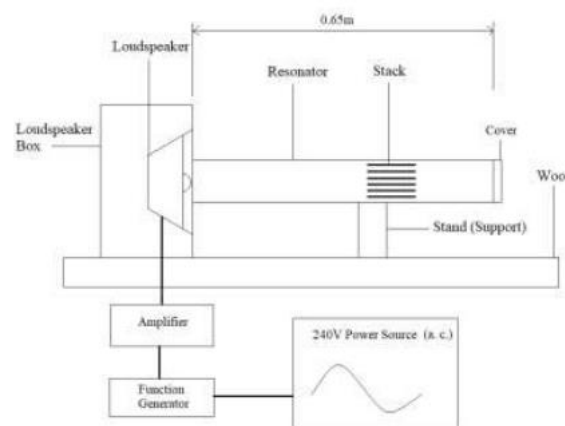


Figure 3: Schematic Diagram of Thermoacoustic Setup

The thermoacoustic refrigerator apparatus consists of resonator, sound driver, driver box, resonator, stack, function generator, and amplifier. The speaker box is made of 30cm x 30 cm x 10 cm customized acrylic box with a 3.1 cm center hole on top surface (30 cm x 30 cm) and 20 cm x 20 cm lockable door at the bottom surface (30 cm x

30 cm). The resonator is made from acrylic tube with 3.5 cm outer diameter, 3.1cm inner diameter, and 0.65 m length. The acrylic material has thermal conductivity,  $k$  in range of  $0.187 \text{ W m}^{-1} \text{ K}^{-1}$  to  $0.209 \text{ W m}^{-1} \text{ K}^{-1}$  and specific heat,  $C_p$  in range of  $1.46 \text{ J g}^{-1} \text{ }^\circ\text{C}^{-1}$  to  $2.16 \text{ J g}^{-1} \text{ }^\circ\text{C}^{-1}$ .

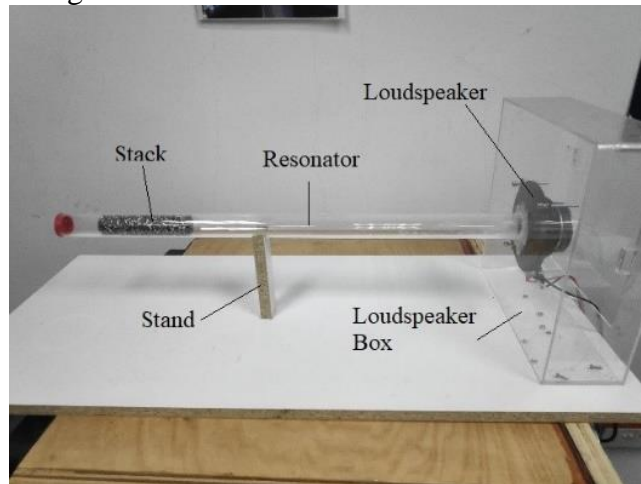


Figure 4: Experimental Thermoacoustic Laboratory Rig

By considering the portability factor, it is considered as too long and therefore, it needs to be cut down to a shorter length of 0.65 m (quarter wavelength). This corresponds to an operation parameter of 133.46 Hz of flow frequency. The sound driver used in the thermoacoustic refrigerator is a used car loudspeaker of Hyundai i10 2008. The loudspeaker's maximum power is 300 W. The cross-section of the 3D printed acrylonitrile butadiene styrene (ABS) stack is initially drawn by using SolidWorks software and saved in stereolithography (STL) format so that CubePro 3D printer software can read the drawing. The cross-section of the ABS stack is as shown in Figure 5. Its area is  $5.04 \text{ cm}^2$  which gives a porosity of 0.3326. The acoustic wave number is calculated by formula,  $J = 2\pi / \lambda$  and for a resonator with a 0.65 m long (quarter wavelength), the acoustic wave number,  $J$  is  $2.42 \text{ m}^{-1}$ .

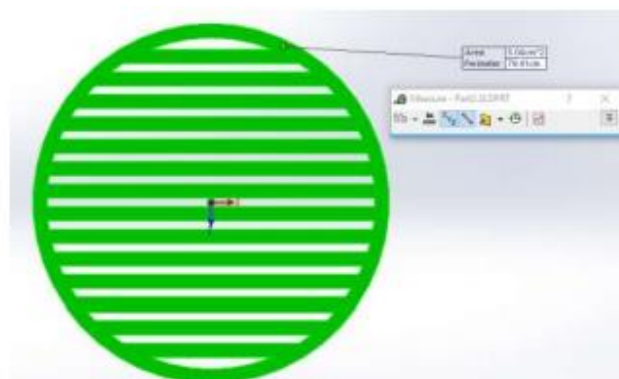


Figure 5: Cross-section of 3D Printed ABS Stack

The amplifier used in this thermoacoustic refrigerator apparatus is Flepcher FLPMT1201 while the function generator used in the thermoacoustic refrigerator apparatus is MCP SG1005. They are fabricated and assembled by using appropriate tools such as table saw, silicone, screws, nuts, et cetera. The instruments used to

measure the temperature and velocity of the thermoacoustic standing wave inside the resonator are the PicoLog Data Logger TC 08 with association with PicoLog 6 software and SENTRY ST-730 hot wire as shown in Figure 6 (a) and (b). The thermocouple used is type K thermocouples as shown in Figure 3.6 (c). Since the hot wire is more sensitive and accurate, the hot wire is used to calibrate the thermocouple readings.

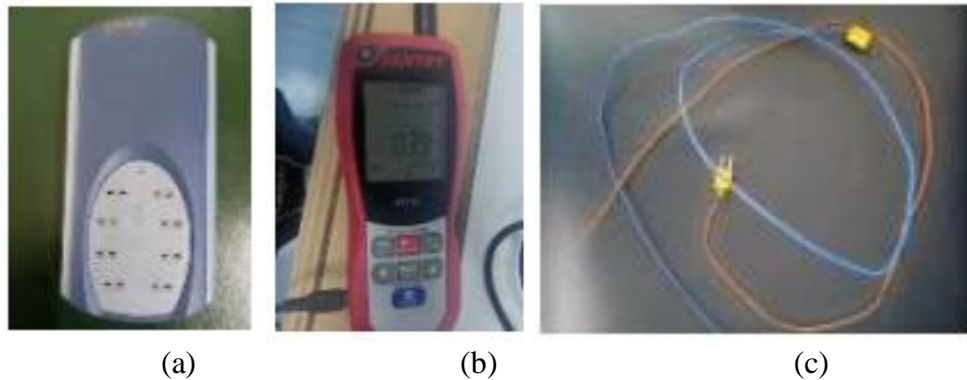


Figure 6: (a) PicoLog Data Logger TC 08, (b) SENTRY ST-730 Hot Wire and (c) Type K Thermocouples

Thermoacoustic refrigerator as shown earlier in Figure 4 was used for implementing an experiment. There are two types of stack; 3D-printed ABS stack and stainless-steel scrubber stack and they are used in the experiment to obtain different temperature reading for comparison purpose. The operating parameters, gas parameters and stack parameters for thermoacoustic refrigerator's parameters are summarized and listed in Table 1 for three-dimensional (3D) acrylonitrile butadiene styrene (ABS) printed stack and Table 2 for stainless-steel scrubber stack. The calculation is based on the formulas in section 1.

Most of the operating parameters are according the optimized characteristics. However, due to limitation of CubePro 3D printer, the plate thickness was set to 1.2 mm. the ABS and stainless-steel scrubber materials are supplied by manufacturer without any specification details. Their thermal properties in terms of specific heat,  $C_p$  and thermal conductivity,  $k$  is therefore assumed.

Table 1: Thermoacoustic Refrigerator's Parameter (3D-Printed ABS Stack)

Operating Parameters		Gas Parameters	
Quarter Wavelength, $\lambda / 4$	0.65 m	Speed of Sound, $a$	347 m s <sup>-1</sup>
Wavelength, $\lambda$	2.6 m	Thermal Conductivity, $k$	0.02566 W m <sup>-1</sup> K <sup>-1</sup>
Acoustic Wave Number, $J$	2.42 m <sup>-1</sup>	Thermal Penetration Depth, $\delta_k$	0.233 mm
Frequency, $f$	133.45 Hz	Specific Heat, $C_p$	1007 J kg <sup>-1</sup> K <sup>-1</sup>
Mean Pressure, $P_m$	101 kPa	Mean density, $\rho_m$	1.176 kg m <sup>-3</sup>
Mean Temperature, $T_m$	300 K	Gas Displacement, $\zeta$	0.47 m
Stack Parameters (ABS)			
Stack Length, $L_s$		0.04 m	
Stack Center Position, $x_s$		0.43 cm	
Thermal Conductivity, $k$		0.195 W m <sup>-1</sup> K <sup>-1</sup>	
Specific Heat, $C_p$		1420 J kg <sup>-1</sup> K <sup>-1</sup>	
Spacing, $2y_o$		0.75 mm	
Plate Thickness		1.2 mm	
Stack Diameter, $d_i$		3.1 cm	
Porosity, $B$		0.3326	

Table 2: Thermoacoustic Refrigerator's Parameter (Stainless Steel Scrubber Stack)

Operating Parameters		Gas Parameters	
Quarter Wavelength, $\lambda / 4$	0.65 m	Speed of Sound, $a$	347 m s <sup>-1</sup>
Wavelength, $\lambda$	2.6 m	Thermal Conductivity, $k$	0.02566 W m <sup>-1</sup> K <sup>-1</sup>
Acoustic Wave Number, $J$	2.42 m <sup>-1</sup>	Thermal Penetration Depth, $\delta_k$	0.233 mm
Frequency, $f$	133.45 Hz	Specific Heat, $C_p$	1007 J kg <sup>-1</sup> K <sup>-1</sup>
Mean Pressure, $P_m$	101 kPa	Mean density, $\rho_m$	1.176 kg m <sup>-3</sup>
Mean Temperature, $T_m$	300 K	Gas Displacement, $\zeta$	0.47 m
Stack Parameters (ABS)			
Stack Length, $L_s$		0.12 m	
Stack Center Position, $x_s$		0.53 mm	
Thermal Conductivity, $k$		15 W m <sup>-1</sup> K <sup>-1</sup>	
Specific Heat, $C_p$		500 J kg <sup>-1</sup> K <sup>-1</sup>	
Stack Diameter, $d_i$		3.1 cm	
Porosity, $B$		0.748	

## 2.2 Computational Fluid Dynamics (CFD) simulation

ANSYS computational fluid dynamics (CFD) software is used for two dimensional simulation of thermoacoustic refrigerator with 3D printed ABS stack.

Figure 7 shows the geometry drawing of the CFD model. A “MultiZone Quad/Tri” mesh method is applied for mesh.

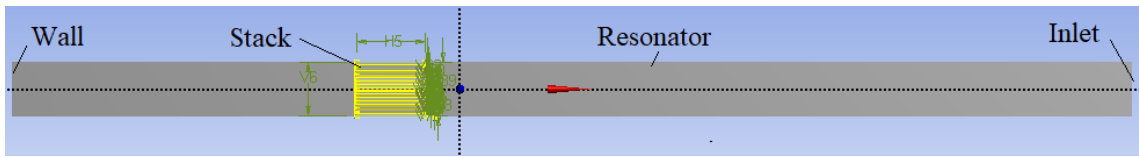


Figure 7: 2D Geometry Drawing in ANSYS

The model used pressure-based solver, absolute velocity formulation, transient time, and planar two-dimensional (2D) space with gravitational acceleration acted on negative  $y$  direction,  $g = -9.81 \text{ m s}^{-2}$  and floating operating pressure of 101,325 Pa. In the models' material setup, there are two materials defined which are air as a working medium and acrylonitrile butadiene styrene (ABS) as the stack's material. The specific heat,  $C_p$  and thermal conductivity,  $k$  of the air were set using polynomial function as shown in Equations (7) and (8), respectively. The correlation coefficient,  $R^2$  of Equation (7) and (8) are 0.99961 and 0.99993 respectively.

$$C_p = 1.9327 \times 10^{-10} T^4 - 7.9999 \times 10^{-7} T^3 + 1.1407 \times 10^{-3} T^2 - 4.4890 \times 10^{-1} T + 1.0575 \times 10^3 \quad (7)$$

$$k = 1.5207 \times 10^{-11} T^3 - 4.8574 \times 10^{-8} T^2 + 1.0184 \times 10^{-4} T - 3.9333 \times 10^{-4} \quad (8)$$

The viscosity of air was set using power-law formula. The density,  $\rho$ , specific heat,  $C_p$ , and thermal conductivity,  $k$  of ABS are  $1215 \text{ kg m}^{-3}$ ,  $1.42 \text{ kJ kg}^{-1} \text{ K}^{-1}$ , and  $0.195 \text{ W m}^{-1} \text{ K}^{-1}$  respectively. The air was set as an ideal gas for this case and  $T$  is the temperature of air. The mass flux is at  $0.588 \text{ kg m}^{-2}$  amplitude with  $90^\circ$  phase difference to the pressure and the flow frequency is 133.45 Hz. The velocity of the air is measured by the SENTRY hot wire anemometer and the value was recorded as  $0.5 \text{ m s}^{-1}$  and this value is used to calculate the mass flux amplitude. In the solution methods configuration, Pressure-Implicit with Splitting of Operators (PISO) scheme was used for dealing with large number of time steps as it would run up to more than 1,000 time steps for each case while others are following the default configurations. Calculation is run at  $7.5 \times 10^{-6} \text{ s}$  of time step size where 1,000 number of time steps is needed to complete one wave cycle for a flow frequency of 133.45 Hz and a flow period of 7.5 ms.

### 3.0 RESULTS AND DISCUSSIONS

The results are discussed through analysis related to the temperature drop obtained through the thermoacoustic setup. In addition, the numerical model is used to produce the pressure and velocity distribution along the resonator of the thermoacoustic apparatus. These are presented in two subsections to separate the findings of the experimental results from the findings of the numerical results.

#### 3.1 Experimental results

Two different stacks were used for the experiment which are acrylonitrile butadiene styrene (ABS) and stainless-steel scrubber and their respective operating parameters were as discussed earlier using Tables 1 and 2. Figure 8 shows graph for

temperature at two end points of three-dimension (3D) printed ABS stack against time. Temperature at one end of the stack is presented by blue line while the temperature at another end is given by the red line. Temperature drop is observed at one end of the stack (red-line) after approximately 4 minutes of operation. The temperature drop between the two ends is sustained for about 25 minutes before the temperature different becomes smaller again. This probably happen because of the absence of heat exchanger to help the system in sustaining the obtained temperature difference.

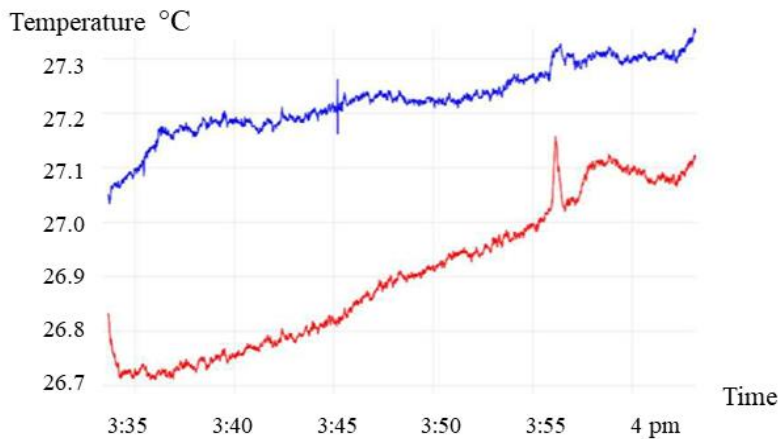


Figure 8: Graph of temperature at two end points of 3D-Printed ABS stack against time

Figure 9 shows a graph of temperature at two ends of stack against time when the stainless-steel scrubber is used as a stack within the same resonator. The stack is now a 12 cm long stainless-steel scrubber as compared to the earlier used of a 4 cm long 3D-printed ABS stack with a stack center position,  $x_s = 0.53$  cm. When ABS stack is used, the highest temperature gradient recorded is  $0.9$  °C which was measured using type-K thermocouple that is connected to PicoLog TC 08 signal conditioner. The highest temperature gradient recorded using scrubber as stack is  $0.6$  °C. The curve of the graph against temperature in stainless steel scrubber stack is more stable compared to the 3D-printed ABS stack because the flow is steadier due to higher porosity. It is shown that the thermoacoustic effect of stainless-steel scrubber stack is more stable than the ABS stack as the graph of temperature against time graph in stainless-steel is more likely uniform than ABS.

However, the temperature difference created across the stack is not high enough because optimization of parameters was not done before the experiment is carried out. Nevertheless, the results show that temperature different was successfully achieved between the two ends of the stack inside the resonator. The temperature different is expected to be bigger if the rig is built at optimum condition.

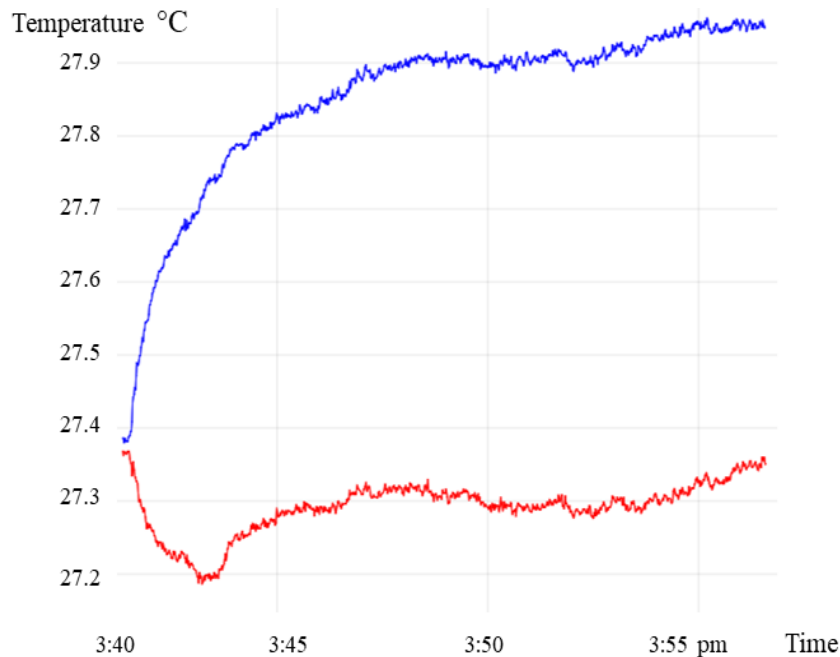


Figure 9: Graph of temperature at two end points of stainless-steel scrubber stack against time

### 3.2 Computational fluid dynamics (CFD) results

Velocity changed with time at the center of the computational domain for different mesh density are as shown in Figure 10. The low mesh density is the mesh with low mesh element while the high mesh density is the mesh with high mesh element which has doubled number of divisions of all edge sizing.

After the mesh independency is checked, the simulation is proceeded to next phase, which is verification of the model. The verification method is to obtain the velocity profile at the centre of the model and compare the simulated velocity profile with the theoretical velocity profile. The solver setting is also described earlier as can be found in subsection 3.2. Since the amplitude of velocity at the inlet is experimentally measured as  $0.5 \text{ m s}^{-1}$ , the antinode pressure,  $P_a$  can be obtained from calculation and it is found to be 204.04 Pa by using the equations Equation (5) and Equation (6). Therefore, the drive ratio is 0.2% for the resonator apparatus that functioned at a frequency of 133.45 Hz and a length of the 0.65 m of the quarter wavelength.

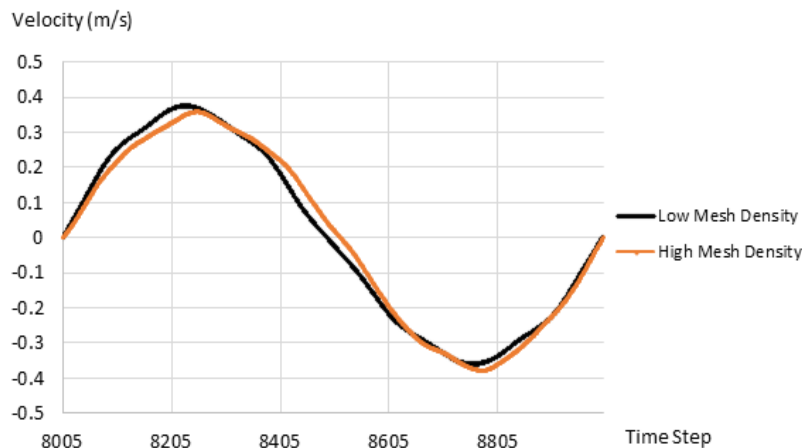


Figure 10: Velocity at the centre of the model for different mesh densities

Figure 11 shows the  $x$ -velocity comparison between the simulated and calculated amplitude results at a point located in the centre of the model.

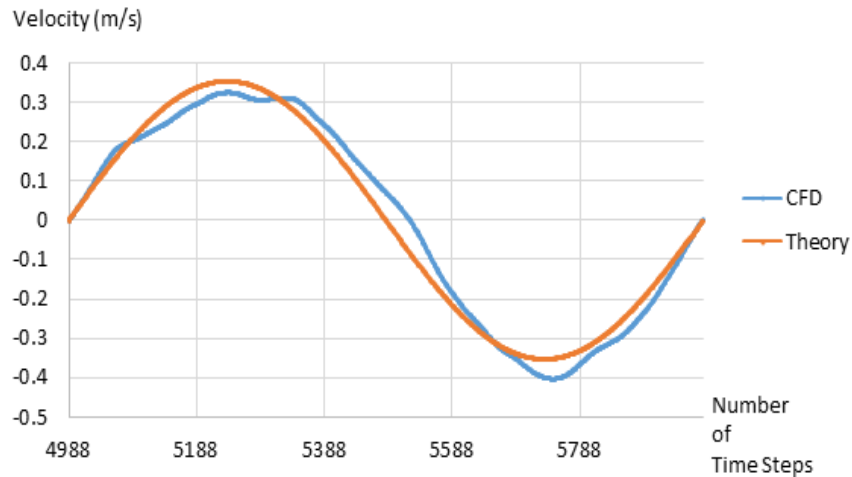


Figure 11: Comparison of  $x$ -velocity between the theoretical and simulation results

Table 3 shows the percentage of error by comparing the theoretical calculated result and the simulated result.

Table 3: Percentage of error of amplitude

Amplitude	Theoretical Value (m s <sup>-1</sup> )	Simulation Value (m s <sup>-1</sup> )	Percentage of Error (%)
Maximum	0.324752	0.35372	8.15
Minimum	-0.40379	-0.35357	14.20

A graph of pressure amplitude against axial direction is plotted as shown in Figure 12. The maximum temperature at the antinode is 218.88 Pa and if it is compared to the theoretical calculation, the value from numerical model differs from the theoretical prediction by 7.27%. Based on the numerical results, it can be concluded that the air particles are vibrating in a range of 0 Pa to 218.88 Pa of pressure in the resonator environment.

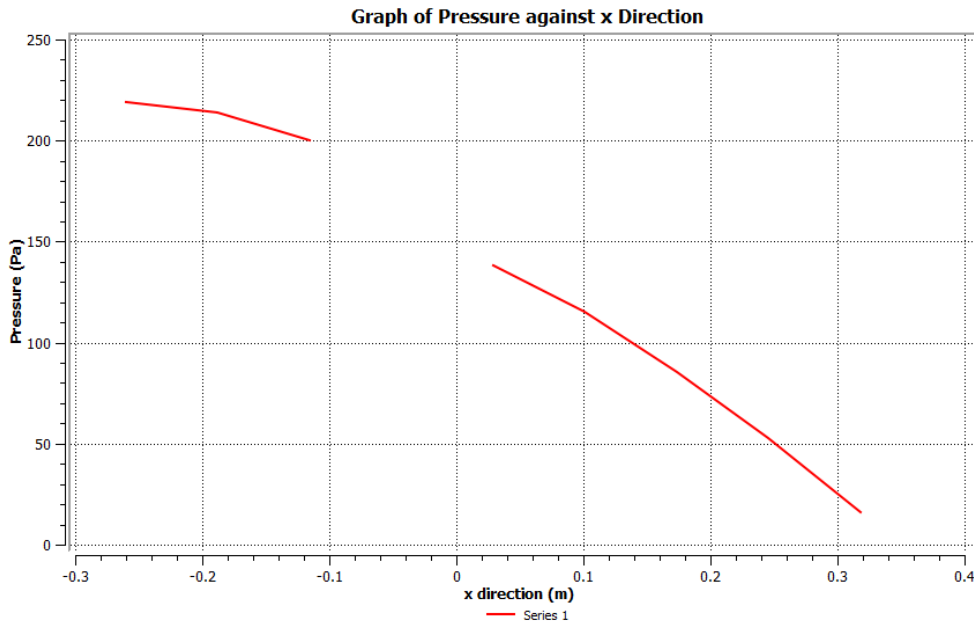


Figure 12: Graph of pressure along  $x$  direction with inlet wall located at the right end.

The temperature across axial direction of the resonator is also discussed. The temperature data is captured at the time step of 8,524. Figure 13 and Table 4 show the graph of temperature against  $x$  direction, and average temperature at both end points of ABS stack respectively.

With reference to Figure 13, the environment temperature for the fluid is 300 K. As the acoustic wave passes through the stack, there is a visible temperature increment at the other end of the stack. The effect of temperature drops is not strong due to parameters which was not optimized, the unsteady state condition of the flow, and the low drive ratio. Along the  $x$  direction, there is a temperature increment from inlet boundary to wall boundary from 299.01 K to 300.07 K.

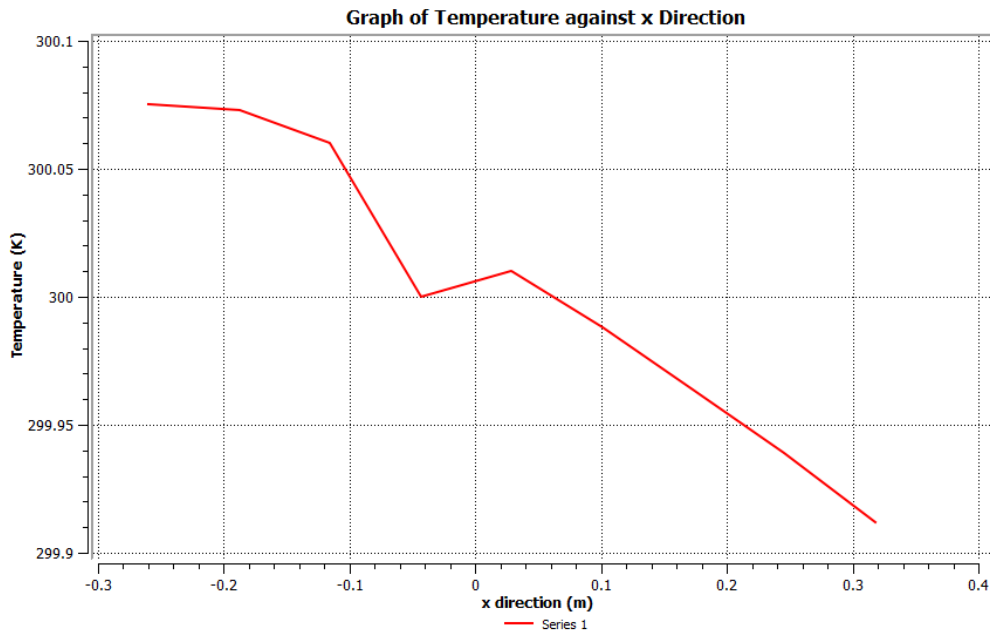


Figure 13: Graph of temperature along  $x$  direction with inlet wall located at the right end.

Two points named as point 1 and point 2 are created in the Cartesian coordinate of  $(-0.02, 0.000975)$  and  $(-0.06, 0.000975)$  in meter. The points are at the two points of stack ends near the gap. Although the temperature differences recorded is 1 K and the acoustic effect is not strong, but this shows that the principle of thermoacoustic is feasible as there is temperature different observed at the two ends of the stack and similar observation was also gained from experimental result as reported earlier in subsection 3.1 where a temperature drop of approximately  $1\text{ }^{\circ}\text{C}$  was recorded.

Table 4: Average temperature at both end points of ABS stack

Probe	Average Temperature (K)
Point 1 $(-0.02, 0.000975)$	301
Point 2 $(-0.06, 0.000975)$	302

Figure 14 shows the graph of the velocity against  $x$  direction. The wave particles at each of the points along the  $x$ -direction vibrate in sinusoidal patterns as was shown earlier in Figure 11. However, as particles move from inlet boundary to the wall boundary at the hard end of the resonator, the amplitude of velocity of the wave particles decreases as it gets closer to the hard end of the resonator following the

standing wave criterion.

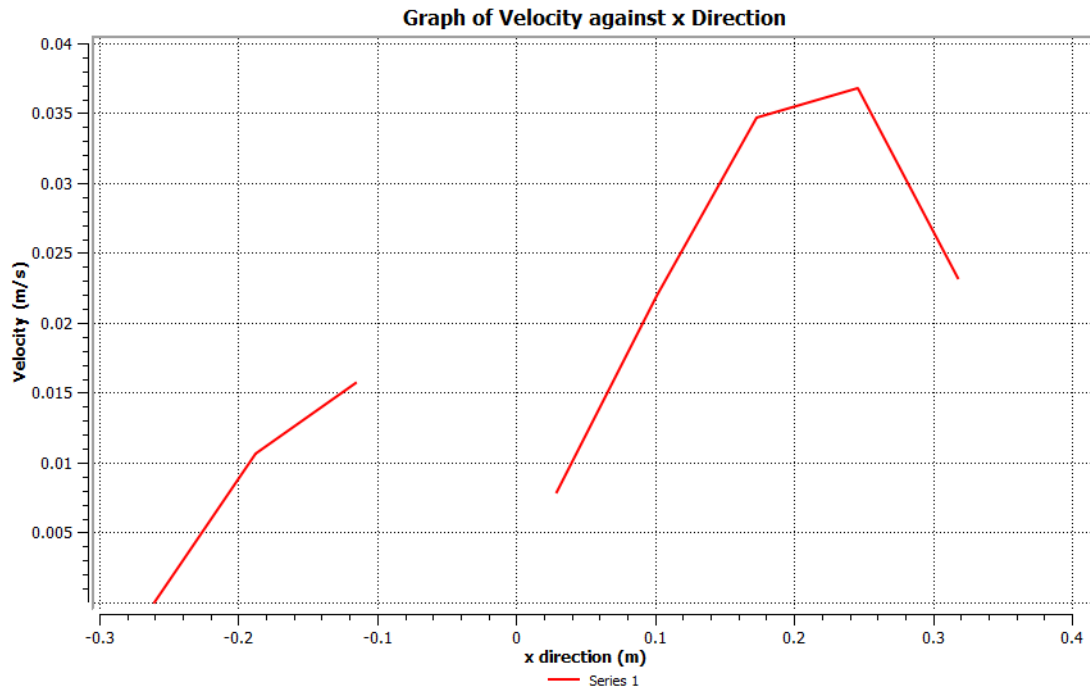


Figure 14: Graph of velocity along  $x$  direction with inlet wall located at the right end.

Hence, it is observable that the velocity of the air particles along  $x$  direction is decreasing from inlet boundary (maximum  $x$ ) and hit zero at the hard end (minimum  $x$ ) of the resonator while the air particles in each point along the  $x$  direction before reaching the hard end vibrate at their amplitude along their orientation line.

#### 4.0 CONCLUSIONh

An experimental test rig was built and a CFD model was solved for a low frequency range thermoacoustic environment. The temperature difference across the both ends of the stack was discussed by comparing the temperature drops at the stack ends. From experimental result, it is shown that a small temperature difference of  $0.9\text{ }^{\circ}\text{C}$  were recorded for the ABS stack while the CFD simulation predicts a temperature difference of  $1\text{ }^{\circ}\text{C}$ . The low temperature difference was obtained due to non-optimised conditions of the thermoacoustic environment. Amongst the parameters that need to be optimised are the resonance frequency, stack's dimension, stack's location (Swift, 2001), (Zolpakar, 2016), (Ibrahim et al., 2011). A bigger temperature difference is expected should the rig be operated at optimised condition and at higher operating conditions (Swift, 2001). Nevertheless, the study shows that a preliminary stage of thermoacoustic rig and CFD models were succesfully developed and further investigation should be carried out to increase the performance to an acceptable level.

## **5.0 ACKNOWLEDGEMENT**

This work has been carried out using facilities at Universiti Teknikal Malaysia Melaka.

## **6.0 REFERENCES**

- Dyatmika, H. S., Achmadin, W. N., Murti, P., Setiawan, I. & Utomo, A. B. S. (2015). Development of the Thermoacoustic Refrigerator System Using a Stack made of some Stainless Steel Mesh and a Hot Heat Exchanger. *Indonesian Journal of Physics*, 26(01). 5 - 8.
- Ibrahim, A., Arafa, N. & Khalil, E., (2011). Geometrical optimization of thermoacoustic heat engines. In: *Proceedings of the Forty-ninth AIAA Aerospace Sciences Meeting including the New Horizons Forum and Aerospace Exposition*.
- Mohd Saat, F. A. Z. & Jaworski, A. J. (2013). Oscillatory Flow and Heat Transfer Within Parallel-plate Heat Exchangers of Thermoacoustic Systems. *Proceeding of the World Congresson Engineering III*.
- Rosli, N. A., Hasan, R., Alkahari, M. R. & Tokoroyama, T. (2017, November 17). Effect of process parameters on the geometrical quality of ABS polymer lattice structure. *Proceedings of SAKURA Symposium on Mechanical Science and Engineering 2017*, pp. 3-5.
- Swift, G. (2001). *Theromoacoustics: A unifying perspective for some engines and refrigerators*. Zhurnal Eksperimental'noi i Teoreticheskoi Fiziki (Fifth Draf). Los Alamos National Laboratory.
- Zolpakar, N. A., Mohd-Ghazali, N. & Hassan, E. F. M. (2016). Performance analysis of the standing wave thermoacoustic refrigerator: A review. *Renewable and Sustainable Energy Reviews*. Elsevier, 54, pp. 626-634. doi: 10.1016/j.rser.2015.10.0